AIAA JOURNAL
Vol. 44, No. 2, February 2006

Aeroelastic Response of Composite Aircraft Swept Wings Impacted by a Laser Beam

Gian Mario Polli*
University of Rome "La Sapienza," 00184 Rome, Italy
Liviu Librescu†
Virginia Polytechnic Institute and State University, Blacksburg, Virginia 24061-0219
and
Franco Mastroddi‡
University of Rome "La Sapienza," 00184 Rome, Italy

A closed-form solution for the thermoaeroelastic response of an aircraft swept wing made of advanced composite materials and exposed to a thermal impact generated by a laser beam is presented. For the aircraft wing, an advanced one-dimensional structural model that includes a number of nonclassical effects, such as transverse shear, warping inhibition, and thermoelastic anisotropy of constituent materials, is developed. It is supposed that the wing is immersed in an incompressible flowfield whose speed is below the flutter critical speed of the system. The solution of the problem has been obtained analytically in the space–time Laplace transform domain. Within this approach, the problem is reduced to the solution of an algebraic equation system in the transformed kinematical unknowns that is afterward inverted in the physical space. Although confined to the dynamic aeroelastic response, the approach of the dynamic response can provide important information on the conditions yielding the occurrence of the flutter instability.

Nomenclature

$\mathcal{A}$	=	wing cross-sectional area
$\boldsymbol{A}, \boldsymbol{B}, \boldsymbol{C}, \boldsymbol{D}, \boldsymbol{E}, \boldsymbol{F}, \boldsymbol{G}$	=	aerodynamic matrices [Eq. (49)]
a	=	dimensionless position of elastic axis, x_0/b
$B_{ij}^{(m,n)}$, $F_i^{(m,n)}$, $I^{(m,n)}$, $S_{ij}^{(m,n)}$	=	generalized stiffness, force, mass, and stress quantities of order (m, n)
b, l	=	semichord and semispan, respectively, m
C_1, C_2, D	=	geometric moments of inertia
$\boldsymbol{c}$	=	vector of natural boundary conditions [Eq. (51)]
c_t	=	specific heat
$\boldsymbol{e}_i$	=	Cartesian base vectors
$\boldsymbol{f}$	=	load vector
$\tilde{f}_{\tilde{2}}(x_2, s)$, $\hat{f}(p, t)$, $\tilde{f}(p, s)$	=	Laplace transform of $f(x_2, t)$, with respect to time, space variable x_2, and with respect to both variables, respectively
g, h, θ, β	=	warping m^{-1}, plunge m, twist angle, and wing-section rotation state-space variables
H	=	wing thickness, m
$\tilde{\boldsymbol{H}}$	=	aeroelastic operator matrix [Eq. (57)]
$\boldsymbol{K}, \boldsymbol{L}, \boldsymbol{M}, \boldsymbol{P}$	=	stiffness matrices
k_1, k_3	=	thermal conductivities in the plane of isotropy and normal to it, respectively
$\mathcal{L}, \mathcal{M}$	=	sectional aerodynamic lift and moment
p, s	=	Laplace transform variables associated to their physical counterparts x_2 and t, respectively
$\boldsymbol{q}$	=	heat density vector, W/m^2
R	=	shear flexibility ratio
R, S	=	boundary-condition matrices [Eq. (51)]
T	=	temperature field, K
t	=	dimensional time variable, s
x_i	=	Cartesian coordinates, $i = 1, 2, 3$
$\boldsymbol{y}$	=	wing state-space vector
δ_1	=	tracer identifying warping effects
∂	=	domain boundary
$\Theta_{ij}^{(m,n)}$, $\phi_i^{(m,n)}$, $\psi_i^{(m,n)}$	=	generalized external moments [Eq. (23)]
Λ	=	wing sweep angle
$\lambda_{pqr}, \boldsymbol{\phi}_{pqr}(\boldsymbol{x})$	=	eigenvalues and eigenfunctions of Laplacian operator related to temperature field in body [Eqs. (34) and (35)]
ρ, ρ_∞	=	material and air density, kg/m^3
τ_0	=	time window width of heat flux input [Eq. (68)]
$\varphi(t)$	=	Wagner function
$\omega_{1_b}, \omega_{1_t}$	=	first bending and first torsion natural frequencies, rad/s
$\dot{}$	=	derivative with respect to time
$'$	=	derivative with respect to x_2

Subscripts

A	=	aerodynamic load
c, nc	=	circulatory and noncirculatory counterparts of the indicated aerodynamic quantity
M	=	mechanical external loads
n	=	quantity normal to leading edge
T	=	thermal load

Presented as Paper 2004-2046 at the AIAA/ASME/ASCE/AHS/ASC 45th Structures, Structural Dynamics, and Materials Conference, Palm Springs, CA, 19–22 April 2004; received 4 February 2005; revision received 15 August 2005; accepted for publication 13 October 2005.

*Postdoctoral Fellow, Department of Aerospace Engineering and Astronautics; gianmario.polli@uniroma1.it.
†Professor, Engineering Science and Mechanics Department; librescu@vt.edu.
‡Associate Professor, Department of Aerospace Engineering and Astronautics; franco.mastroddi@uniroma1.it.

I. Introduction

In this paper, a formulation and closed-form solution for the aeroelastic response of an aircraft swept wing made of advanced composite materials, whose upper surface is impacted by a laser beam, is presented. The expression of the temperature field within the body has been obtained using the Green's function method. Because, via a laser beam, one can easily apply a highly intense heat density vector on the wing surfaces that can have a detrimental implication on the wing aeroelastic behavior and because the specialized literature is void of such studies, the aerothermoelastic response of aircraft wings impacted by a laser beam is investigated in this paper. For the aircraft wing, an advanced structural model is developed by converting the equations of the three-dimensional elasticity theory to the one-dimensional equations and by including the effects of transverse shear, warping restraint, and thermoelastic anisotropy of the constituent materials. It is supposed that the wing is immersed in a subsonic incompressible flow whose speed is lower than the flutter critical speed of the system. To generate the aerothermoelastic governing equations, a generalization of a previously developed structural model for advanced aircraft swept wings[1–4] made up of monoclinic multilayered composites is carried out. For computational purposes, and toward highlighting the effects of a number of physical and geometrical parameters, the case of a rectangular single-layered swept wing composed of a transversely isotropic material is considered. Given its exceptional features in the thermal protection of aerospace structures,[5,6] the pyrolytic graphite that features thermomechanical transversely isotropic properties is considered in the wing modeling. Because of the time dependence of the thermal field and that herein the aeroelastic response is addressed, the unsteady aerodynamic theory of lifting surfaces has been considered in the time domain. Then the problem is analytically solved in a double Laplace transform space domain, where both the space and time coordinates are converted to their Laplace variable space counterparts. Within this approach, the problem is reduced to the solution of an algebraic problem in the transformed kinematical unknowns, and the solution in the physical space and time domain was obtained via an inverse double Laplace transform. Although this paper is confined to the study of the dynamic aeroelastic response in the linear framework, important information regarding the conditions of occurrence of the flutter instability can be obtained. In the presentation and discussion of results, special emphasis has been placed on the effects of transverse shear flexibility, sweep angle, laser power time dependence, and flight speed on aeroelastic response. To the authors' best knowledge, in spite of its actuality and practical importance, the problem treated in this paper has not been yet addressed in the specialized literature.

II. Geometry and Kinematical Considerations

The wing structure is modeled as a platelike body with appropriate internal constraints: In particular, it is assumed that the wing structure is rigid in the chordwise and thickness directions. Therefore, given an orthogonal Cartesian frame with orthogonal unit vectors $\{\boldsymbol{e}_1, \boldsymbol{e}_2, \boldsymbol{e}_3\}$, with $\boldsymbol{e}_1$ and $\boldsymbol{e}_2$ in the chordwise and spanwise directions, respectively (Fig. 1), and coordinate axes $\{x_1, x_2, x_3\}$, the following representation for the displacement field has been assumed[1,4]:

$$\boldsymbol{u}(x_1, x_2, x_3, t) = x_3\theta(x_2, t)\boldsymbol{e}_1 + \{v_2(x_2, t) - x_3[\beta(x_2, t) - \delta_1 x_1 g(x_2, t)]\}\boldsymbol{e}_2 + \{h(x_2, t) - [x_1 - x_0(x_2, t)]\theta(x_2, t)\}\boldsymbol{e}_3 \tag{1}$$

where $\theta(x_2, t)$ denotes the twist angle of the wing about its pitching axis, $\beta(x_2, t)$ identifies the flexural angle about the chordwise direction, $g(x_2, t)$ represents the warping displacement, $h(x_2, t)$ denotes the plunging displacement of the wing cross section measured at the elastic axis [positive upward and located at $x_{1e} = x_0(x_2)$; Fig. 1], and δ_1 is a tracer introduced to identify the warping effect.[1] The tracer takes the value 1 or 0 according to whether the warping limitation is incorporated or discarded, respectively: The two resulting formulations are denoted in the following text as free warping (FW) and warping restraint (WR) models, respectively. The geometrical representation of the wing in the spanwise direction is shown in Fig. 1. Collecting the independent displacement components in Eq. (1), one may observe that the total number of unknowns retained into the model is five, and in terms of these five displacement unknowns $(v_2, \beta, g, \theta, h)$ the aeroelastic response analysis under the effect of a thermomechanical load is investigated.

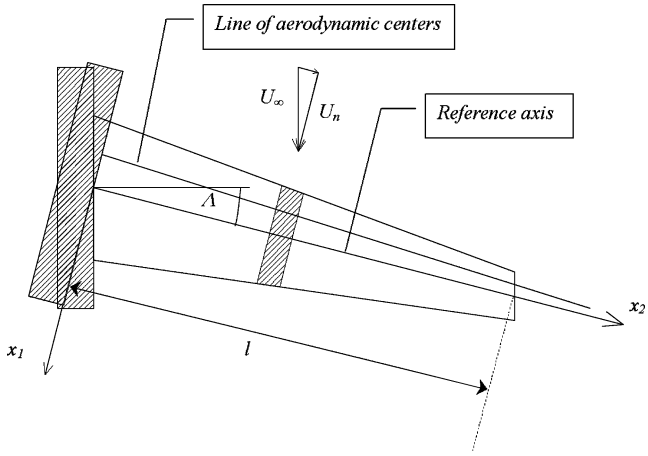

Fig. 1 Geometry of swept wing.

III. Equations of Motion and Boundary Conditions

To obtain the equilibrium equations and the related boundary conditions, the generalized Hamilton's principle has been used. This corresponds to minimization of an energy functional[1,3,7,8] for an arbitrary variation of the admissible generalized displacements. Thus, introducing suitable definitions for the stress moments, moments of inertia, body forces moments, and traction moments of order (m, n), one may obtain five partial differential equilibrium equations in the five displacement unknowns, with as many boundary conditions on each edge. In particular, with $\mathcal{A}$ denoting the cross-sectional area of the wing, the moments of order (m, n) may be defined as

$$S_{ij}^{(m,n)}(x_2, t) := \int_{\mathcal{A}(x_2)} \sigma_{ij}(x_1, x_2, x_3, t) x_1^m x_3^n \, \mathrm{d}x_3 \, \mathrm{d}x_1 \tag{2}$$

$$\left[I^{(m,n)}(x_2, t),\, F_i^{(m,n)}(x_2, t)\right] := \int_{\mathcal{A}(x_2)} \rho(x_1, x_2, x_3, t)[1,\, f_i(x_1, x_2, x_3, t)] x_1^m x_3^n \, \mathrm{d}x_3 \, \mathrm{d}x_1 \tag{3}$$

$$\phi_i^{(m,n)}(x_2, t) := \int_{c(x_2)} \left\{ \left[t_i(x_1, x_2, x_3, t) x_3^n \right]_{x_3 = -H/2} + \left[t_i(x_1, x_2, x_3, t) x_3^n \right]_{x_3 = H/2} \right\} x_1^m \, \mathrm{d}x_1 \tag{4}$$

$$\psi_i^{(m,n)}(t) := \int_{\mathcal{A}(l)} t_i(x_1, x_2, x_3, t) x_1^m x_3^n \, \mathrm{d}x_3 \, \mathrm{d}x_1 \tag{5}$$

where σ_{ij} are the Cartesian components of the Cauchy stress tensor, ρ is the wing mass density per unit wing volume, and f_i and t_i are the Cartesian components of the external body and surface forces, respectively. Given the arbitrary and independent variation of the admissible generalized displacements, the equations of motion are obtained as

$$\delta v_2 : \left(S_{22}^{(0,0)}\right)' + F_2^{(0,0)} - I^{(0,0)}\ddot{v}_2 + I^{(0,1)}\ddot{\beta} - I^{(1,1)}\ddot{g} + \phi_2^{(0,0)} = 0 \tag{6}$$

$$\delta\beta : \left(S_{22}^{(0,1)}\right)' - S_{23}^{(0,0)} + F_2^{(0,1)} - I^{(0,1)}\ddot{v}_2 + I^{(0,2)}\ddot{\beta} - I^{(1,2)}\ddot{g} + \phi_2^{(0,1)} = 0 \tag{7}$$

$$\delta g : \left(S_{22}^{(1,1)}\right)' - S_{23}^{(1,0)} - S_{12}^{(0,1)} + F_2^{(1,1)} - I^{(1,1)}\ddot{v}_2 + I^{(1,2)}\ddot{\beta} - I^{(2,2)}\ddot{g} + \phi_2^{(1,1)} = 0 \tag{8}$$

$$\delta\theta : \left(S_{12}^{(0,1)}\right)' - \left(S_{23}^{(1,0)}\right)' + \left(S_{23}^{(0,0)}\right)' x_0 + F_1^{(0,1)} - F_3^{(1,0)} + F_3^{(0,0)} x_0 - \left(I^{(0,2)} + I^{(2,0)} - 2I^{(1,0)}x_0 + I^{(0,0)}x_0^2\right)\ddot{\theta} + \left(I^{(1,0)} - I^{(0,0)}x_0\right)\ddot{h} - \mathcal{M} - \phi_3^{(1,0)} + x_0\phi_3^{(0,0)} = 0 \tag{9}$$

$$\delta h : \left(S_{23}^{(0,0)}\right)' + F_3^{(0,0)} - I^{(0,0)}\ddot{h} + \left(I^{(1,0)} - I^{(0,0)}x_0\right)\ddot{\theta} + \mathcal{L} + \phi_3^{(0,0)} = 0 \tag{10}$$

where $\mathcal{L}$ and $\mathcal{M}$ are the sectional lift and aerodynamic torque about the reference axis per unit span.

With regard to the boundary conditions, a clamped condition has been assumed at the root, whereas at the tip the following natural boundary conditions have been obtained:

$$\delta v_2 : S_{22}^{(0,0)} = \psi_2^{(0,0)} \tag{11}$$

$$\delta\beta : S_{22}^{(0,1)} = \psi_2^{(0,1)} \tag{12}$$

$$\delta g : S_{22}^{(1,1)} = \psi_2^{(1,1)} \tag{13}$$

$$\delta\theta : S_{12}^{(0,1)} - S_{23}^{(1,0)} + S_{23}^{(0,0)}x_0 = \psi_1^{(0,1)} - \psi_3^{(1,0)} + \psi_3^{(0,0)}x_0 \tag{14}$$

$$\delta h : S_{23}^{(0,0)} = \psi_3^{(0,0)} \tag{15}$$

Note that in Eqs. (6–15) the forces on the boundary surfaces of the wing have been divided into two distinct contributions: One is related to the aerodynamic forces and the other to those resulting from the external time-dependent loads acting on the wing during the operational flight of the flight vehicle, for example, a thermal field or an explosive blast load. Moreover, Eqs. (6–10) constitute a system of five differential equations, each one of second order, whose natural boundary conditions are represented by Eqs. (11–15) in terms of the earlier defined displacement unknowns. Clearly, the discard of the warping restraint leads to a system of four differential equations. Their expressions are not provided here, but the interested reader can find these in Refs. 1–3, which provide a detailed description of this model.

IV. Thermoelastic Constitutive Equations

The present formulation is carried out in the framework of the uncoupled thermoelasticity.[9] For this reason, the temperature will enter into the problem by means of the constitutive relations. In particular, in the framework of linear thermoelasticity, the Hooke–Duhamel constitutive equations have been considered. To show how the temperature explicitly enters into the problem, the expression of the stress moments of order (m, n) [Eqs. (2)] for a generic composite structure, in terms of the displacement unknowns and generalized thermal moments, are supplied:

$$S_{22}^{(0,0)} = B_{22}^{(0,0)}u_2' - B_{22}^{(0,1)}\beta' + B_{26}^{(0,1)}(g + \theta') + B_{22}^{(1,1)}g' - \Theta_2^{(0,0)} \tag{16}$$

$$S_{22}^{(0,1)} = B_{22}^{(0,1)}u_2' - B_{22}^{(0,2)}\beta' + B_{26}^{(0,2)}(g + \theta') + B_{22}^{(1,2)}g' - \Theta_2^{(0,1)} \tag{17}$$

$$S_{22}^{(1,1)} = B_{22}^{(1,1)}u_2' - B_{22}^{(1,2)}\beta' + B_{26}^{(1,2)}(g + \theta') + B_{22}^{(2,2)}g' - \Theta_2^{(1,1)} \tag{18}$$

$$S_{23}^{(0,0)} = B_{44}^{(0,0)}(-\beta + h' + (x_0\theta)') + B_{44}^{(1,0)}(g - \theta') \tag{19}$$

$$S_{23}^{(1,0)} = B_{44}^{(1,0)}(-\beta + h' + (x_0\theta)') + B_{44}^{(2,0)}(g - \theta') \tag{20}$$

$$S_{12}^{(0,1)} = B_{62}^{(0,1)}u_2' - B_{62}^{(0,2)}\beta' + B_{66}^{(0,2)}(g + \theta') + B_{62}^{(1,2)}g' - \Theta_6^{(0,1)} \tag{21}$$

where $B_{ij}^{(m,n)}$ and $\Theta_i^{(m,n)}$, for $i, j = 2, 4, 6$, are the generalized stiffness quantities and thermal moments, respectively, defined by

$$B_{ij}^{(m,n)}(x_2) := \int_{\mathcal{A}(x_2)} x_1^m x_3^n Q_{ij}(x_3)\,\mathrm{d}x_3\,\mathrm{d}x_1 \tag{22}$$

$$\Theta_i^{(m,n)}(x_2, t) := \int_{\mathcal{A}(x_2)} x_1^m x_3^n \gamma_i(x_3) T(x_j, t)\,\mathrm{d}x_3\,\mathrm{d}x_1 \tag{23}$$

where $Q_{ij}(x_3)$ and $\gamma_i(x_3)$ are the transformed elastic and thermal expansion coefficients associated with the composite structure of the wing. Note that in our approach, the distribution of the composite material has been defined as a pointwise variation of the material properties across the wall thickness. In the case of multilayered composite structures, this representation reduces to a piecewise one.

V. Thermal Field

As was stated in the Introduction, the case of a laser beam impacting the upper surface of the wing is considered. Mathematically, the problem may be stated in terms of the following system of equations[9–12]:

$$\mathrm{Div}(\boldsymbol{K}\nabla T) - \rho c_t \frac{\partial T}{\partial t} = 0, \qquad \text{for} \qquad \boldsymbol{x} \in \mathcal{B}, \qquad t \in \mathcal{T} \tag{24}$$

$$\boldsymbol{K}\nabla T \cdot \boldsymbol{n} = \boldsymbol{q} \cdot \boldsymbol{n}, \qquad \text{for} \qquad \boldsymbol{x} \in \mathcal{S}_U, \qquad t \in \mathcal{T} \tag{25}$$

$$\nabla T \cdot \boldsymbol{n} = 0, \qquad \text{for} \qquad \boldsymbol{x} \in \partial\mathcal{B}/\mathcal{S}_U, \qquad t \in \mathcal{T} \tag{26}$$

$$T = 0, \qquad \text{for} \qquad \boldsymbol{x} \in \partial\mathcal{B}, \qquad t = 0 \tag{27}$$

where $T(\boldsymbol{x}, t)$ is the temperature field, $\boldsymbol{K}$ is the thermal conductivity tensor,[13] $\boldsymbol{n}$ is the external normal to the surface body, $\boldsymbol{q}$ is the external heat density vector impacting the wing, and $\mathcal{B}$ and $\mathcal{T}$ denote, respectively, the space and time domains. To determine analytically the temperature field within the body, a Green's approach has been applied (see Ref. 14). In particular, when ϕ_{pqr} denotes the eigenfunctions and λ_{pqr} the corresponding eigenvalues of the Laplacian operator for the problem under consideration, the temperature field may be written[7,8,10]

$$T(\boldsymbol{x}, t) = \sum_{p,q,r=0}^{\infty} \frac{\phi_{pqr}(\boldsymbol{x})}{\rho c_t} \int_{\mathcal{S}_U} \phi_{pqr}(\boldsymbol{x}^*) \int_0^t \exp\left[-\frac{k_1\lambda_{pqr}}{\rho c_t}(t - t^*)\right] \times \boldsymbol{q}(\boldsymbol{x}^*, t^*) \cdot \boldsymbol{n}(\boldsymbol{x}^*, t^*)\,\mathrm{d}t^*\,\mathrm{d}\mathcal{S} \tag{28}$$

Note that, using Eq. (28), one can establish an explicit relation between the temperature field and the unknown components of the displacement field. Indeed, using the following linear approximation of the unit normal to the deformed upper surface of the wing[8]:

$$\boldsymbol{n}(\boldsymbol{x}, t) \cong \boldsymbol{e}_3 - h'(x_2, t)\boldsymbol{e}_2 + \theta(x_2, t)\boldsymbol{e}_1 \tag{29}$$

and substituting Eq. (29) into Eq. (28), one may express the temperature field as the sum of three contributions:

$$T(\boldsymbol{x}, t) = T_1(\boldsymbol{x}, t) + T_2(\boldsymbol{x}, t) + T_3(\boldsymbol{x}, t) \tag{30}$$

where $T_1(\boldsymbol{x}, t)$ represents the perturbation of the temperature field due to the torsional rotation θ of the wing and is given by

$$T_1(\boldsymbol{x}, t) = \sum_{p,q,r=0}^{\infty} \frac{\phi_{pqr}(\boldsymbol{x})}{\rho c_t} \int_{\mathcal{S}_U} \phi_{pqr}(\boldsymbol{x}^*) \int_0^t \exp\left[-\frac{k_1\lambda_{pqr}}{\rho c_t}(t^* - t)\right] \times q_1(\boldsymbol{x}^*, t^*)\theta\left(x_2^*, t^*\right)\mathrm{d}t^*\,\mathrm{d}\mathcal{S} \tag{31}$$

and $q_1(\boldsymbol{x}, t)$ is the component of the heat density vector in the x_1 direction. Similarly, $T_2(\boldsymbol{x}, t)$ represents the perturbation of the temperature field due to the flexural rotation h' of the wing and is given by

$$T_2(\boldsymbol{x}, t) = -\sum_{p,q,r=0}^{\infty} \frac{\phi_{pqr}(\boldsymbol{x})}{\rho c_t} \int_{\mathcal{S}_U} \phi_{pqr}(\boldsymbol{x}^*) \times \int_0^t \exp\left[-\frac{k_1 \lambda_{pqr}}{\rho c_t}(t^* - t)\right] q_2(\boldsymbol{x}^*, t^*) h'\left(x_2^*, t^*\right) \mathrm{d}t^* \, \mathrm{d}\mathcal{S} \quad (32)$$

where $q_2(\boldsymbol{x}, t)$ is the component of the heat density vector in the x_2 direction. Finally, $T_3(\boldsymbol{x}, t)$ represents the main temperature field in the body due to the heat flux, $q_3(\boldsymbol{x}, t)$, in the direction of the undeformed unit normal $\boldsymbol{e}_3$ and is given by

$$T_3(\boldsymbol{x}, t) = \sum_{p,q,r=0}^{\infty} \frac{\phi_{pqr}(\boldsymbol{x})}{\rho c_t} \int_{\mathcal{S}_U} \phi_{pqr}(\boldsymbol{x}^*) \int_0^t \exp\left[-\frac{k_1 \lambda_{pqr}}{\rho c_t}(t^* - t)\right] \times q_3(\boldsymbol{x}^*, t^*) \, \mathrm{d}t^* \, \mathrm{d}\mathcal{S} \quad (33)$$

To adapt these formulations to the specific case considered in this paper, a parallelepiped geometry has been considered for the wing in conjunction with the heat flux constant along the spanwise x_2 direction.[9,15] For this special geometry, the associated thermal eigenproblem gives[9,10]

$$\phi_{pqr}(\boldsymbol{x}) = \frac{2\sqrt{2}}{\sqrt{2bl\sqrt{k_1/k_3}H}} \times \cos\left(\frac{p\pi}{2b}x_1\right) \cos\left(\frac{q\pi}{l}x_2\right) \cos\left(\frac{r\pi}{H}x_3\right) \quad (34)$$

$$\lambda_{pqr} = -\left[\left(\frac{p\pi}{2b}\right)^2 + \left(\frac{q\pi}{l}\right)^2 + \left(\frac{r\pi}{\sqrt{k_1/k_3}H}\right)^2\right] \quad (35)$$

and, as a result, Eq. (33) reduces to

$$T(x_3, t) = \frac{8\sqrt{k_3}}{\sqrt{k_1}\rho c_t H} \sum_{r=0}^{\infty} (-1)^r \cos\frac{r\pi x_3}{H} \exp\left(-\frac{k_3 r^2 \pi^2}{\rho c_t H^2} t\right) \times \int_0^t \exp\left(\frac{k_3 r^2 \pi^2}{\rho c_t H^2} t^*\right) q(t^*) \, \mathrm{d}t^* \quad (36)$$

where ρ is the mass density and $q(t)$ is the x_3 component of the heat density vector. In Fig. 2 a possible deformed configuration of the wing structure considered in the applications is shown. Here the heat density vector is symbolized by $\boldsymbol{q}(x_2, t)$, whereas the normal is denoted by $\boldsymbol{n}(x_2, t)$. Finally, note that in the present paper the numerical results are limited to a completely uncoupled formulation with the thermal field acting as an external load. In particular, the expression of the temperature field employed in the applications is that provided by Eq. (33), with the further assumptions of a parallelepiped geometry for the body and of the constancy of the heat density vector in the spanwise direction.

VI. Unsteady Aerodynamic Model

In this section, the unsteady aerodynamic loads corresponding to an incompressible unsteady two-dimensional flowfield over the wing, taking into account the effect of the sweep angle, are presented. For the problem at hand, given the time dependence of the thermal loads, a time-domain representation of the theory of lifting surfaces, analogous to that reported in Refs. 16 and 17 and applied in Ref. 18, has to be used.

In accordance with Ref. 17, the sectional lift and the aerodynamic torque may be expressed as the sum of two contributions, namely, of the circulatory and noncirculatory ones. Specifically, for the unsteady lift, one may have

$$\mathcal{L}(x_2, t) = \mathcal{L}_c(x_2, t) + \mathcal{L}_{\mathrm{nc}}(x_2, t) \quad (37)$$

where

$$\mathcal{L}_c(x_2, t) = -2\pi\rho_\infty U_n b_n \int_{-\infty}^{t} \varphi(t - \hat{t}) \left\{ \ddot{h} - \left(\frac{b_n}{2} - a b_n\right)\ddot{\theta} + U_n\left[-\dot{\theta} + \tan\Lambda\left(\dot{h}' - \left(\frac{b_n}{2} - a b_n\right)\dot{\theta}'\right)\right]\right\} \mathrm{d}\hat{t} \quad (38)$$

$$\mathcal{L}_{\mathrm{nc}}(x_2, t) = \pi\rho_\infty b_n^2 [-\ddot{h} + U_n\dot{\theta} - b_n a\ddot{\theta} - U_n \tan\Lambda(\dot{h}' + a b_n\dot{\theta}')] \quad (39)$$

where $\varphi(t)$ is the Wagner's function given by (see Ref. 16)

$$\varphi(t) := \frac{1}{2\pi} \int_{-\infty}^{+\infty} \frac{C(\omega)}{j\omega} e^{j\omega t} \, \mathrm{d}\omega \quad (40)$$

and $C(\omega)$ is the Theodorsen function.

Similarly, for the aerodynamic moment, one has

$$\mathcal{M}(x_2, t) = \mathcal{M}_c(x_2, t) + \mathcal{M}_{\mathrm{nc}}(x_2, t) \quad (41)$$

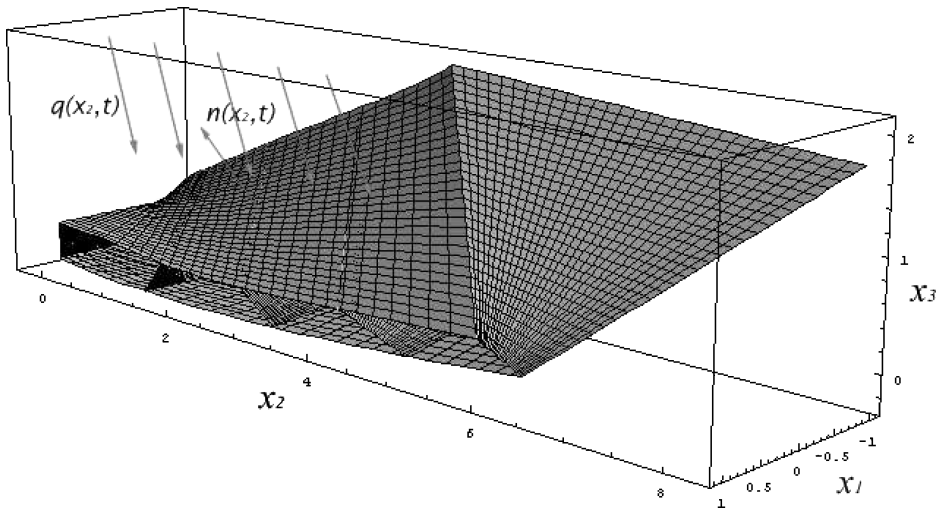

Fig. 2 Deformed configuration of wing structure exposed to external heat flux.

where

$$\mathcal{M}_{\rm nc}(x_2,t)=2\pi\rho_\infty U_n b_n^2\left(\frac{1}{2}+a\right)\int_{-\infty}^{t}\varphi(t-\hat{t})\left\{-\ddot{h}+U_n\dot{\theta}\right.$$

$$\left.-U_n\tan\Lambda\dot{\theta}'+b_n\left(\frac{1}{2}-a\right)(\ddot{\theta}+U_n\tan\Lambda\dot{\theta}')\right\}\mathrm{d}\hat{t} \tag{42}$$

$$\mathcal{M}_c(x_2,t)=b_n\left(\frac{1}{2}+a\right)\mathcal{L}_c \tag{43}$$

VII. Solution Methodology

This section is devoted to the development of the solution procedure enabling one to solve the present aerothermoelastic problem [Eqs. (6–10)]. With respect to a rectangular single-layered wing, made of a transversely isotropic material uniformly distributed in the spanwise direction, a number of stiffness quantities such as, for example, $B_{ij}^{(1,n)}=B_{ij}^{(m,1)}=B_{26}^{(m,n)}=0$, vanish [Eq. (22)]. The remaining nonzero stiffness quantities can be expressed as

$$B_{22}^{(0,0)}:=\mathcal{A}Q_{22},\qquad B_{22}^{(0,2)}:=C_1Q_{22},\qquad B_{22}^{(2,2)}:=DQ_{22}$$

$$B_{44}^{(0,0)}:=\mathcal{A}Q_{44},\qquad B_{44}^{(2,0)}:=C_3Q_{44},\qquad B_{66}^{(0,2)}:=C_1Q_{66} \tag{44}$$

where $\mathcal{A}$ is the area of the wing cross section, C_1 and C_3 are the geometric moments of inertia with respect to the chordwise and thickness direction, and D is the warping geometric moment, or warping constant of Vlasov (see Ref. 19), respectively, given by

$$[\mathcal{A},C_1,C_3,D]:=\int_{\mathcal{A}}\left[1,x_3^2,x_1^2,x_1^2x_3^2\right]\mathrm{d}x_3\,\mathrm{d}x_1 \tag{45}$$

Moreover, Q_{22}, Q_{44}, and Q_{66} are the nonzero elastic coefficients that, for a transversely isotropic material, are given by

$$Q_{22}:=E/(1-\nu^2),\qquad Q_{44}:=G',\qquad Q_{66}:=E/2(1+\nu) \tag{46}$$

With the preceding expressions, the governing equations (6–10) are recast in a suitable compact form introducing a state-space vector $\boldsymbol{y}$ whose components are the ordered displacement unknowns

$$y_1:=u_2,\qquad y_2:=\beta,\qquad y_3:=g,\qquad y_4:=\theta,\qquad y_5:=h \tag{47}$$

Substituting Eqs. (44–47) into Eqs. (16–21) and then in the equilibrium equations (6–10) yields

$$\boldsymbol{K}\boldsymbol{y}''+\boldsymbol{L}\boldsymbol{y}'+\boldsymbol{P}\boldsymbol{y}+\boldsymbol{M}\ddot{\boldsymbol{y}}=\boldsymbol{f}_A+\boldsymbol{f}_T+\boldsymbol{f}_M \tag{48}$$

where the primes and the overdots denote the derivatives with respect to x_2 and t, respectively; $\boldsymbol{K}$, $\boldsymbol{L}$, $\boldsymbol{P}$ are the stiffness matrices whose expression is reported in Refs. 7 and 8; and $\boldsymbol{f}_A$ is the vector of aerodynamic loads, $\boldsymbol{f}_T$ is the vector of thermal load, and $\boldsymbol{f}_M$ is the vector of mechanical loads resulting from the external time-dependent loads acting on the wing such as explosive blast loads or sonic boom pulses. In particular, substituting Eqs. (47) into Eqs. (37–43), one has

$$\boldsymbol{f}_A(\boldsymbol{y},\dot{\boldsymbol{y}},\ddot{\boldsymbol{y}},\boldsymbol{y}',\dot{\boldsymbol{y}}',t,x_2)=\boldsymbol{A}\ddot{\boldsymbol{y}}+\boldsymbol{B}\dot{\boldsymbol{y}}+\boldsymbol{C}\boldsymbol{y}'+\boldsymbol{D}\dot{\boldsymbol{y}}'$$

$$+\boldsymbol{E}\int_0^t\varphi(t-\hat{t})\ddot{\boldsymbol{y}}(\hat{t})\,\mathrm{d}\hat{t}+\boldsymbol{F}\int_0^t\varphi(t-\hat{t})\dot{\boldsymbol{y}}(\hat{t})\,\mathrm{d}\hat{t}$$

$$+\boldsymbol{G}\int_0^t\varphi(t-\hat{t})\dot{\boldsymbol{y}}'(\hat{t})\,\mathrm{d}\hat{t} \tag{49}$$

where the matrices $\boldsymbol{A}$, $\boldsymbol{B}$, $\boldsymbol{C}$, $\boldsymbol{D}$, $\boldsymbol{E}$, $\boldsymbol{F}$, and $\boldsymbol{G}$, whose expressions are not supplied in the paper, can be obtained by comparing Eq. (49) with Eqs. (37–43). The boundary conditions, associated with Eq. (48) and obtained by performing the same transformations on Eqs. (11–15) at the wing root ($x_2=0$) and tip ($x_2=l$) are

$$\boldsymbol{y}=0\qquad\text{for}\qquad x_2=0 \tag{50}$$

$$\boldsymbol{R}\boldsymbol{y}'+\boldsymbol{S}\boldsymbol{y}=c\qquad\text{for}\qquad x_2=l \tag{51}$$

Note that c includes the thermal moments, which, for the particular temperature distribution considered here, appear only in the boundary conditions.

Applying the Laplace transform with respect to time

$$L_t[\cdot]:=\int_0^\infty\cdot\,e^{-st}\,\mathrm{d}t$$

to Eqs. (48–51) and assuming zero initial conditions, one obtains

$$\boldsymbol{K}\tilde{\boldsymbol{y}}''+\tilde{\boldsymbol{N}}(s,U_n)\tilde{\boldsymbol{y}}'+\tilde{\boldsymbol{Q}}(s,U_n)\tilde{\boldsymbol{y}}=\tilde{\boldsymbol{f}}_T+\tilde{\boldsymbol{f}}_M \tag{52}$$

where the tilde, $L_t[\cdot]\equiv\tilde{\cdot}$, denotes a Laplace transform with respect to time, s is the time counterpart in the Laplace domain, and

$$\tilde{\boldsymbol{N}}(s,U_n):=\boldsymbol{L}-\boldsymbol{C}-s\boldsymbol{D}-s\tilde{\varphi}\boldsymbol{G} \tag{53}$$

$$\tilde{\boldsymbol{Q}}(s,U_n):=\boldsymbol{P}+s^2(\boldsymbol{M}-\boldsymbol{A}-\tilde{\varphi}\boldsymbol{E})-s(\boldsymbol{B}+\tilde{\varphi}\boldsymbol{F}) \tag{54}$$

where $\tilde{\varphi}$ is the Laplace transform of the Wagner's function and it is given by [see Eq. (40)]

$$\tilde{\varphi}:=L_t[\varphi(t)]=\tilde{C}(s)/s \tag{55}$$

Performing the Laplace transform with respect to space

$$L_{x_2}[\cdot]:=\int_0^\infty\cdot\,e^{-px_2}\,\mathrm{d}x_2$$

denoting with the overhat ($L_{x_2}[\cdot]\equiv\hat{\cdot}$) the corresponding Laplace transform quantities, and recalling that the wing is considered to be clamped at the root, that is, for $x_2=0$, one has

$$\hat{\tilde{\boldsymbol{y}}}(p,s)=\left[p^2\boldsymbol{K}+p\tilde{\boldsymbol{N}}(s,U_n)+\tilde{\boldsymbol{Q}}(s,U_n)\right]^{-1}[\hat{\tilde{\boldsymbol{f}}}_T(p,s)$$

$$+\hat{\tilde{\boldsymbol{f}}}_M(p,s)+\boldsymbol{K}\tilde{\boldsymbol{y}}'(0,s)] \tag{56}$$

where p is the space variable counterpart in the Laplace domain.

Let us define

$$\hat{\tilde{\boldsymbol{H}}}(p,s,U_n):=\left[p^2\boldsymbol{K}+p\tilde{\boldsymbol{N}}(s,U_n)+\tilde{\boldsymbol{Q}}(s,U_n)\right]^{-1} \tag{57}$$

which may be regarded as the aeroelastic operator. Thus, Eq. (56) may be cast as

$$\hat{\tilde{\boldsymbol{y}}}(p,s)=\hat{\tilde{\boldsymbol{H}}}(p,s,U_n)[\hat{\tilde{\boldsymbol{f}}}_T(p,s)+\hat{\tilde{\boldsymbol{f}}}_M(p,s)]$$

$$+\hat{\tilde{\boldsymbol{H}}}(p,s,U_n)\boldsymbol{K}\tilde{\boldsymbol{y}}'(0,s) \tag{58}$$

Performing the inverse Laplace transform with respect to space, one has

$$\tilde{\boldsymbol{y}}(x_2,s)=\int_0^{x_2}\tilde{\boldsymbol{H}}(\eta,s)\tilde{\boldsymbol{f}}(x_2-\eta,s)\,\mathrm{d}\eta+\tilde{\boldsymbol{H}}(x_2,s)K\tilde{\boldsymbol{y}}'(0,s) \tag{59}$$

and defining the convolution integral

$$\tilde{\boldsymbol{g}}(x_2,s):=\int_0^{x_2}\tilde{\boldsymbol{H}}(\eta,s)\tilde{\boldsymbol{f}}(x_2-\eta,s)\,\mathrm{d}\eta \tag{60}$$

Eq. (59) becomes

$$\tilde{\boldsymbol{y}}(x_2,s)=\tilde{\boldsymbol{g}}(x_2,s)+\tilde{\boldsymbol{H}}(x_2,s)\boldsymbol{K}\tilde{\boldsymbol{y}}'(0,s) \tag{61}$$

and by virtue of Eq. (60), we have

$$\tilde{\boldsymbol{y}}'(x_2,s)=\tilde{\boldsymbol{g}}'(x_2,s)+\tilde{\boldsymbol{H}}'(x_2,s)\boldsymbol{K}\tilde{\boldsymbol{y}}'(0,s) \tag{62}$$

The boundary conditions at the tip [Eq. (51)] are

$$\boldsymbol{R}[\tilde{\boldsymbol{g}}'(l,s)+\tilde{\boldsymbol{H}}'(l,s)\boldsymbol{K}\tilde{\boldsymbol{y}}'(0,s)]+\boldsymbol{S}[\tilde{\boldsymbol{g}}(l,s)+\tilde{\boldsymbol{H}}(l,s)\boldsymbol{K}\tilde{\boldsymbol{y}}'(0,s)]=\tilde{\boldsymbol{c}}(s) \tag{63}$$

thus,

$$\tilde{\boldsymbol{y}}'(0,s)=[\boldsymbol{R}\tilde{\boldsymbol{H}}'(l,s)\boldsymbol{K}+\boldsymbol{S}\tilde{\boldsymbol{H}}(l,s)\boldsymbol{K}]^{-1}\{\tilde{\boldsymbol{c}}(s)-[\boldsymbol{R}\tilde{\boldsymbol{g}}'(l,s)+\boldsymbol{S}\tilde{\boldsymbol{g}}(l,s)]\} \tag{64}$$

Finally, the solution vector still in the Laplace transformed space (with respect to time) may be written as

$$\tilde{\boldsymbol{y}}(x_2,s)=\int_0^{x_2}\tilde{\boldsymbol{H}}(\eta,s)\tilde{\boldsymbol{f}}(x_2-\eta,s)\,\mathrm{d}\eta+\tilde{\boldsymbol{H}}(x_2,s)[\boldsymbol{R}\tilde{\boldsymbol{H}}'(l,s)+\boldsymbol{S}\tilde{\boldsymbol{H}}(l,s)]^{-1}\{\tilde{\boldsymbol{c}}(s)-[\boldsymbol{R}\tilde{\boldsymbol{g}}'(l,s)+\boldsymbol{S}\tilde{\boldsymbol{g}}(l,s)]\} \tag{65}$$

Equation (65) gives the analytic solution in the Laplace time domain of the aeroelastic response to a thermal load of an advanced structural wing model. In connection with Eq. (65), note that the solution of the problem depends on the convolution of the external load (distributed along the span) with the transfer function of the system $\boldsymbol{H}$ and on the loads applied at the wing tip $\boldsymbol{c}$.

VIII. Numerical Results

In this section, results related to the aeroelastic response of a single-layered, uniform, rectangular, swept wing are presented and discussed. In particular, the results have been divided into two parts: one devoted to the validation of the model with respect to that of Goland[20] (see also Ref. 1) and Goland and Luke[21] (see also Ref. 22), and another regarding the aerothermoelastic response. In the first part, the dynamic characteristics of the Goland wing are presented in terms of frequency response functions (FRFs) and of dynamic stability analysis. In this regard, one should notice that consideration of the FRFs permits not only evaluation of the spectrum of eigenmodes appearing in a certain broadband, but also evaluation of how the frequency content is modified as a result of the considered effects. Moreover, the evaluation of the FRFs for various flight speeds permits the identification of the flutter occurrence and of the mode, or of modes that contribute mainly to the response in the flutter condition. In particular, the analysis concerns the comparison of the response within the FW and WR models. In the second part, after the formulation of the assumptions regarding the external heat density vector and the wing material properties, the time histories of the plunging and pitching degrees of freedom, due to the considered thermal excitation, are reported and discussed. Chosen as a reference configuration was that of the straight wing with WR and transverse shear effect included. In the presentation of the results special emphasis has been placed on the effects of the transverse isotropy of the constituent material, sweep angle, transverse shear flexibility, heat flux time variation, and flight speed.

A. Model Validation

The wing model by Goland[20] has been considered as a reference for the validation of the present model. As a result, the following geometrical and dynamic characteristics have been assumed:

$$l=6.096\,\mathrm{m},\qquad b=0.9144\,\mathrm{m},\qquad a=-\tfrac{1}{3}$$

$$x_{\mathrm{c.g.}}=0.2b,\qquad \omega_{1_b}=50\ \mathrm{rad/s},\qquad \omega_{1_t}=87\ \mathrm{rad/s} \tag{66}$$

where l is the midspan, b the midchord measured normally to the trailing edge, a the nondimensional distance (with respect to the midchord) between the aerodynamic center and the elastic center, and $x_{\mathrm{c.g.}}$ is the distance between the center of gravity and the elastic center of the wing. Here ω_{1_b} and ω_{1_t} are, respectively, the first uncoupled bending and torsion angular frequencies of the wing.

By the use of the earlier displayed numerical data and under the assumption that $R=0$ that is, an unshearable model, the dynamics and aeroelastic stability of the wing, featuring FW and WR, have been solved separately. Specifically, Fig. 3 shows the FRFs for the pitch and plunge degrees of freedom for the FW and WR models in still air. Note that consideration of the warping inhibition affects mainly the first torsion frequency, which is increased from the original 95.68 rad/s of the FW coupled model to the 130.75 rad/s of the WR coupled model, but not the bending one, which is slightly increased from the original 48.12 rad/s of the FW coupled model to the 48.78 rad/s of the WR coupled model, a result that is expected due to the constrained nature of this model. The effects of transverse shear flexibility on the first bending and torsion angular frequencies for the two models are reported in Table 1. In this regard, it may be observed that the increase of transverse shear flexibility yields a reduction of both the first bending and torsional natural frequencies. The decay of the first bending frequency of the FW ($\omega_{1,b}^{\mathrm{FW}}$) and WR ($\omega_{1,b}^{\mathrm{WR}}$) models is comparable, whereas the decrease of the first torsion frequency is much more stronger in the WR model ($\omega_{1,t}^{\mathrm{WR}}$) than in the FW model ($\omega_{1,t}^{\mathrm{FW}}$).

Table 1 Transverse shear flexibility effect on first bending and torsion frequencies[a]

$R(:=E/G')$	$\omega_{1,b}^{\mathrm{FW}}$	$\omega_{1,b}^{\mathrm{WR}}$	$\omega_{1,t}^{\mathrm{FW}}$	$\omega_{1,t}^{\mathrm{WR}}$
0	48.12	48.78	95.68	130.75
20	46.52	47.05	93.33	119.20
40	45.05	45.49	91.14	110.58
60	43.72	44.06	89.10	103.88
80	42.47	42.75	87.21	98.52
100	41.35	41.56	85.41	94.12

[a]Radians per second.

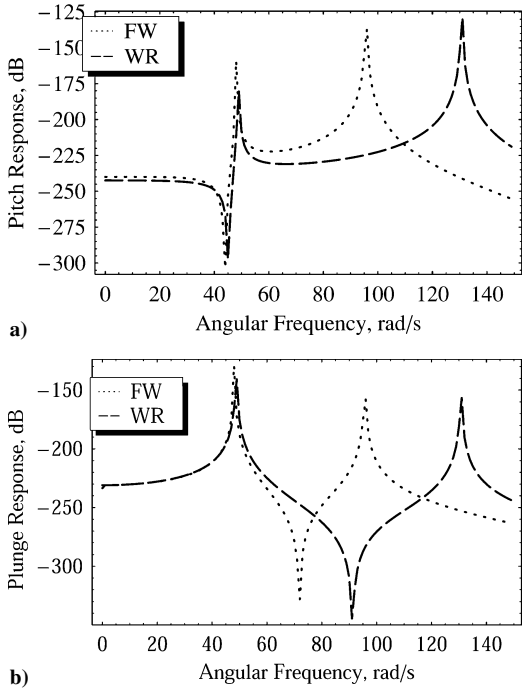

Fig. 3 FRFs of FW and WR models: a) pitching and b) plunging motion.

The aeroelastic stability analysis is shown in Figs. 4 and 5 in terms of the FRFs of plunge and pitch degrees of freedom, respectively. Specifically, Fig. 4 shows the FRFs of the pitch and plunge degrees of freedom for the FW model of the reference straight wing at nine different flight speeds in the range [0, 160] m/s with an increment of 20 m/s at each step. Similarly, Fig. 5 shows the FRFs of the pitch and plunge degrees of freedom for the WR model at 10 different flight speeds in the range [0, 270] m/s with an increment of 30 m/s at each step. Note that when one of the poles of the aeroelastic system lies on the imaginary axis the aeroelastic FRFs tend to infinity at the corresponding frequency of such a pole. The FRFs of the system at various flight speeds can provide important information on the occurrence of static and dynamic aeroelastic instabilities. This

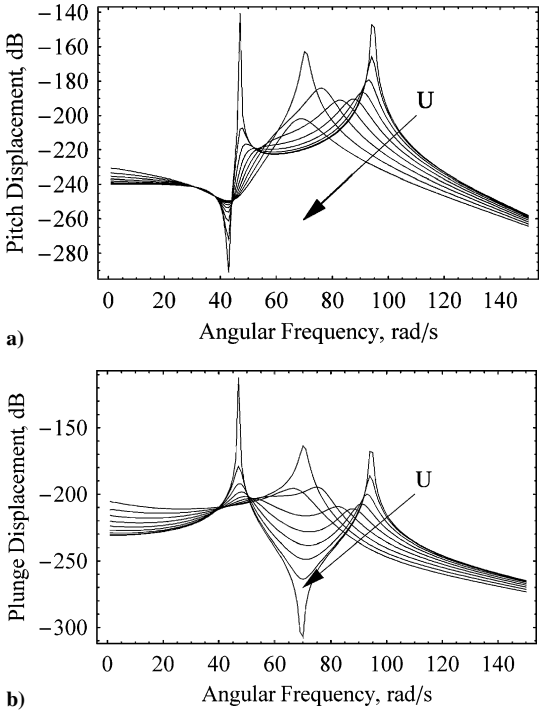

Fig. 4 FRFs of FW model for $0 \le U \le 160$ m/s, $\Lambda = 0$ and $R = 0$, with step of 20 m/s: a) pitching and b) plunging motion.

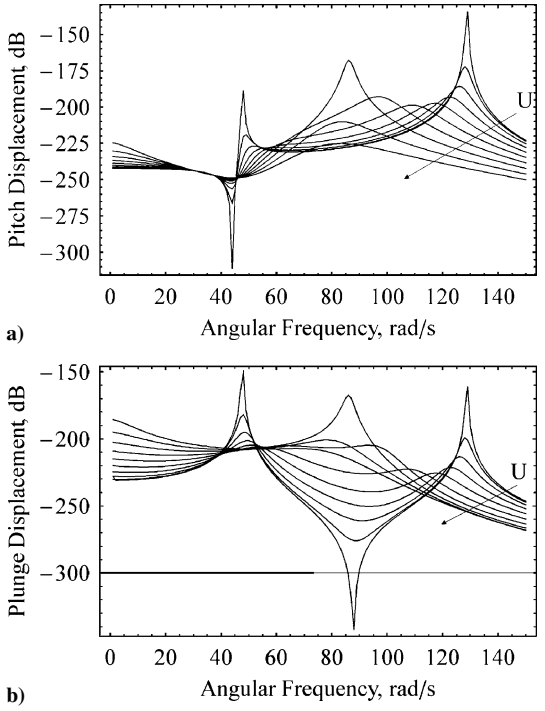

Fig. 5 FRFs of WR model for $0 \le U \le 270$ m/s, $\Lambda = 0$ and $R = 0$, with step of 30 m/s: a) pitching and b) plunging motion.

reasoning may become apparent while observing Figs. 4 and 5. Indeed, in still air the FRFs feature two peaks corresponding to the two natural frequencies of the structure (compare with Fig. 3), whereas at $U = 140$ and 210 m/s, respectively, for the FW and WR unshearable, that is, for $R = 0$, the FRFs exhibit a peak at 70 and 86 rad/s, respectively, indicating that the aeroelastic system is in the proximity of the flutter instability. Finally, note that in extending the range of the flight speed much above the flutter speed, one may find for this particular wing model similar peaks at zero frequency, indicating the occurrence of a static aeroelastic instability or divergence.

Similar indications about the occurrence of the aeroelastic instabilities may also be found by looking at the determinant of the

Table 2 Transverse shear flexibility effect on flutter speed[a] and angular frequency[b]

$R(:= E/G')$	$U^{\mathrm{FW}}_{\mathrm{flutter}}$	$U^{\mathrm{WR}}_{\mathrm{flutter}}$	$\omega^{\mathrm{FW}}_{\mathrm{flutter}}$	$\omega^{\mathrm{WR}}_{\mathrm{flutter}}$
0	136.0	204.9	70.08	86.17
20	133.0	184.1	68.09	79.94
40	129.5	168.7	66.47	75.18
60	127.0	156.7	64.80	71.40
80	124.5	147.3	63.22	68.31
100	122.0	139.6	61.82	65.71

[a]Meters per second. [b]Radians per second.

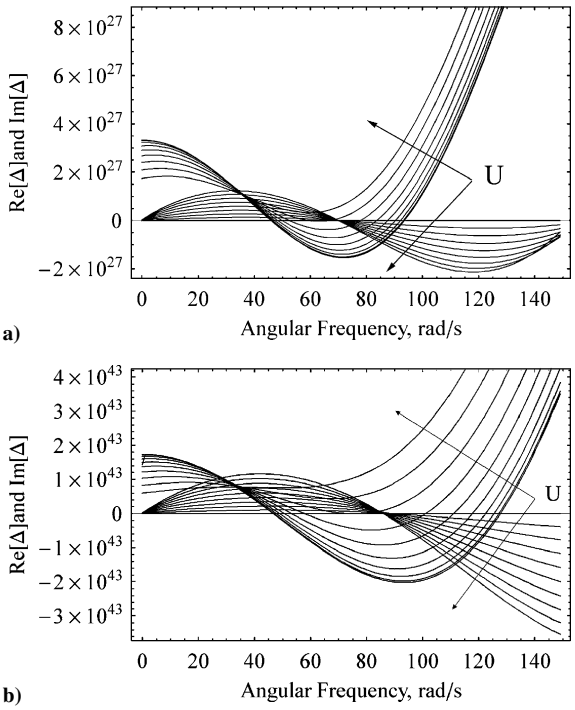

Fig. 6 $\Re[\Delta(\omega)]$ and $\Im[\Delta(\omega)]$ for $0 \le U \le 160$ m/s, $\Lambda = 0$ and $R = 0$, with steps of 20 m/s of a) FW model, and for $0 \le U \le 270$ m/s, $\Lambda = 0$ and $R = 0$, with steps of 30 m/s of b) WR model.

inverse of the aeroelastic operator [Eq. (65)] evaluated on the imaginary axis,

$$\Delta(j\omega, U_n) := \det[R\tilde{H}'(l, j\omega, U_n)K + S\tilde{H}(l, j\omega, U_n)K] \quad (67)$$

Accordingly, Fig. 6 shows the real and imaginary parts of the Δ for several flight speeds in the range [0, 160] m/s and [0, 270] m/s for the FW and WR models, respectively, with an increment of 20 and 30 m/s, respectively, at each step. The aeroelastic instability may be determined when the $\Im(\Delta)$ and $\Re(\Delta)$ are simultaneously zero. In particular, the instability will be static, that is divergence, if this happens at zero frequency and/or dynamic instability, that is, flutter, if this occurs at a nonzero frequency. Before proceeding further, note that the results obtained in terms of flutter speed and flutter frequency, that is, 136 m/s and 70.08 rad/s (Table 2) for the reference model are in very good agreement with the Goland[20] and Goland and Luke[21] exact results, namely, $V_{\mathrm{flutter}} = 137.2$ m/s and $\omega_{\mathrm{flutter}} = 70.65$ rad/s. Although the solution procedure used in this paper is different of that in Ref. 1, the flutter predictions are identical.

To evaluate the effect of the transverse shear flexibility on the aeroelastic behavior of the two models, in Table 2, the flutter speeds and angular frequencies of the FW and WR models for various transverse shear flexibility ratios are reported. Note that the flutter instability appears, in both of the considered wing models, essentially in the torsional mode, and that the WR model is more stable than the FW model. This is because the warping restraint on the root cross section introduces torsion stiffness into the model so that the wing becomes more rigid in twist. Opposite considerations apply

with respect to the transverse shear flexibility effect; in particular, from Tables 1 and 2, it may be observed that the increase of the flexibility ratio yields an attenuation of the effects of the WR such that the WR model for $R = 100$ is almost aeroelastically equivalent to the FW unshearable wing model, that is, for $R = 0$.

B. Aerothermoelastic Response

In this subsection the aerothermoelastic response of the uniform rectangular wing, considered in the preceding section and exposed to a time-dependent laser beam, is presented. Note that due to the uniform distribution of the external heat density flux along the wing span, the thermal excitation intervenes in terms of the boundary conditions, only. The temperature field acting in the body is given by Eq. (36) for a parallelepiped geometry and for a heat density vector constant along the spanwise direction,[9,15] and $q(t)$ is the modulus of the heat density vector (oriented in the x_3 direction) expressed as

$$q(t) = (q_{\max}/2)[1 - \cos 2\pi(t/\tau_0)] \tag{68}$$

for $0 < t < \tau_0$ and zero elsewhere, where its amplitude $q_{\max}$ was fixed to the value 10^7 W/m^2, and τ_0 denotes the time-window width of heat density vector input. Also note that the earlier representation of the heat time dependence is as a reasonable approximation of a typical wideband process as a time-impulsive laser beam may be. (See, for instance, Ref. 12, where a similar but more complicated expression was used to simulate heat deposition by means of a laser pulse.) Moreover, it permits easy variation of the spectral content of the input signal just acting on the time-window width of the signal τ_0 and, thus, excitation of more modes in a certain frequency bandwidth.

Given the preceding considerations, several aeroelastic analyses have been performed. Specifically, chosen as reference configuration is that of a uniform unswept wing incorporating the WR feature (WR model) and the effect of the transverse shear flexibility ($R := E/G' = 100^1$). The effect of the transverse isotropy of the constituent material has been analyzed together with the effects of the external heat period, flight speed, transverse shear flexibility ratio, and sweep angle.

In particular, Fig. 7 shows the time and frequency content of the input signal for four different time periods ($\tau_0 = 0.05$, 0.1, 0.25, and 0.5 s), whose effect has been evaluated in Fig. 8. From Fig. 7, it may be inferred that only for $\tau_0 = 0.05$ s is the external heat input

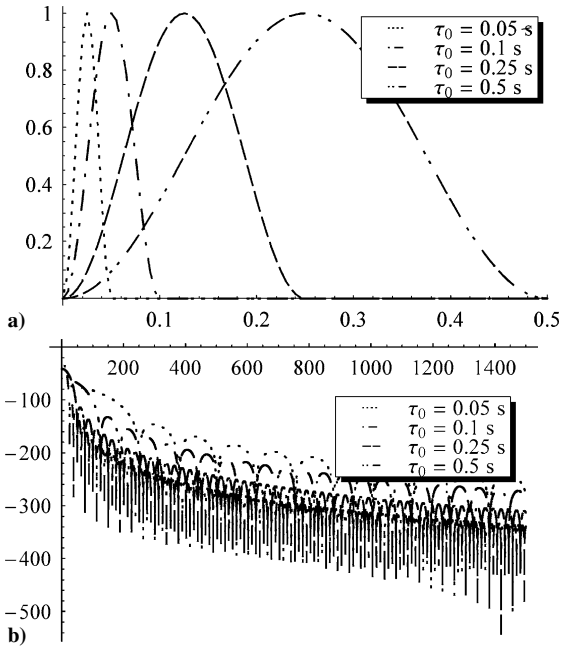

Fig. 7 Content of thermal excitation a) time and b) frequency for selected values of time window of thermal load.

Table 3 Material and aerodynamic reference values used in numerical simulations

Parameter	Value
R	100
ρ_∞, kg/m^3	1.225
U, m/s	100
τ_0, s	0.1
Λ	0
k_3, kg · m/s^3 · K	300

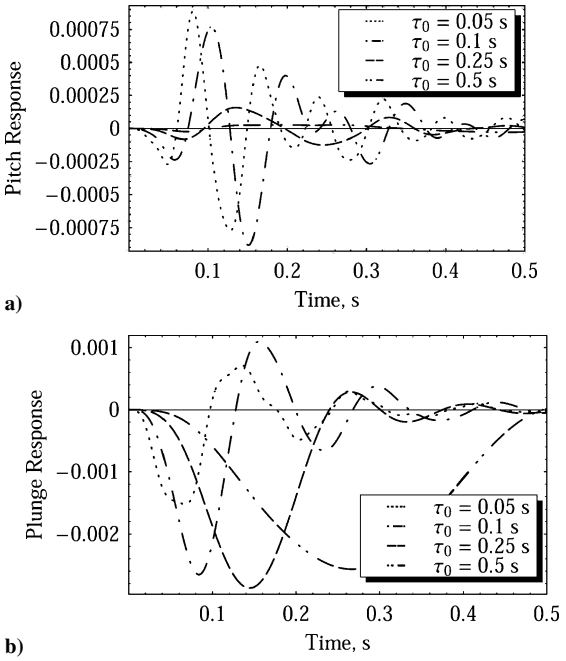

Fig. 8 Effect of time-window width of heat flux input on a) pitch and b) plunge time histories.

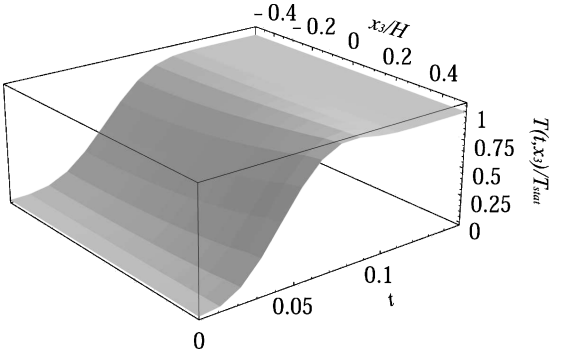

Fig. 9 Temperature field.

capable of exciting wing modes in a wider range of frequencies because for $\tau_0 = 0.05$ s the heat flux is close to a Dirac function in the origin.

In Fig. 9 a three-dimensional plot of the temperature field arising in the body due to the impact of the laser beam is shown for $\tau_0 = 0.1$ s. In particular, the ratio of the temperature field with respect to its stationary value is represented on the ordinate axis as function of time and thickness x_3 coordinate. Indeed, note that, due to the impermeability condition provided by Eq. (26), the temperature after a transient reaches a stationary value.

The reference values of the material and aerodynamic properties chosen in the analysis for the WR model are reported in Table 3. Note that the reference value for the thermal conductivity is that of the pyrolytic graphite in the plane of isotropy as reported in Ref. 23, whereas the specific heat is chosen such that the characteristic thermal time is equal to the characteristic structural one, that is, the

first bending period. Although this choice may appear arbitrary, it is particularly useful in evaluating the thermally induced vibrations of the wing as discussed in Ref. 9. Indeed, the importance of the inertia effects increases as the ratio of these two characteristic times becomes smaller; in contrast, as this ratio increases, the inertia forces disappear and the static solution remains valid only.

To illustrate the effect of the anisotropy of the material constituents, in Fig. 10 the time histories of the pitch and plunge displacements in the reference configuration are compared to those pertinent to other two different choices of thermal conductivity in the thickness direction. In particular, for $k_3 = k_1/100$, a condition typical of a pyrolytic graphite material results.[23] From Fig. 10, it is apparent that the consideration of a much smaller thermal conductivity in the thickness direction yields an attenuation of the response. This result is not surprising if one recalls Eq. (36), where the ratio

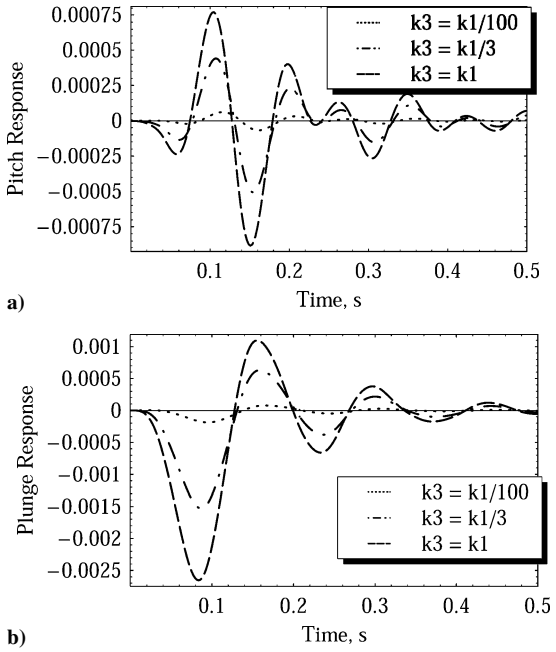

Fig. 10 Effect of thermal conductivity ratio on a) pitch and b) plunge time histories.

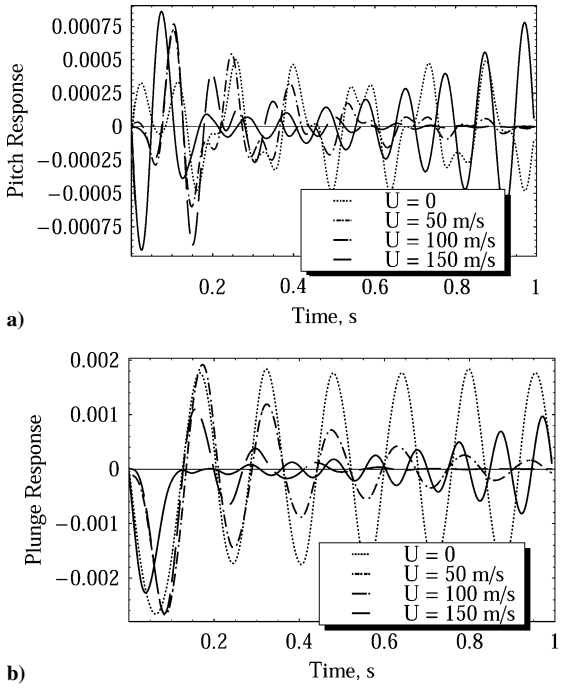

Fig. 11 Effect of flight speed, $\Lambda = 0$, on a) pitching and b) plunging motions.

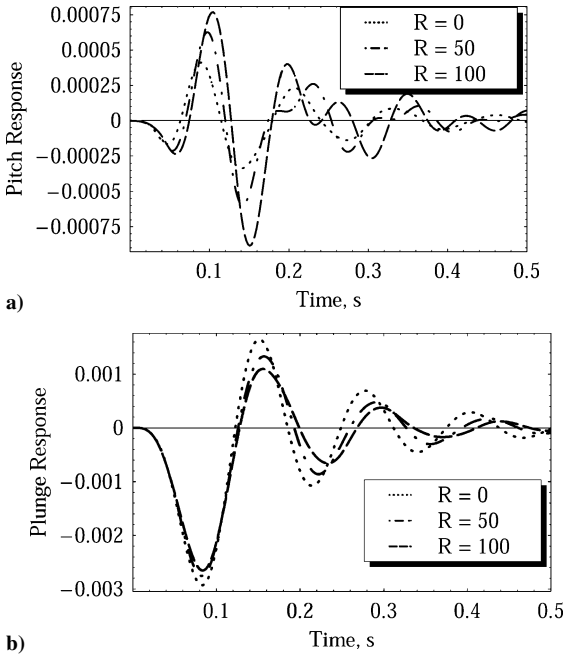

Fig. 12 Effect of transverse shear: a) pitching and b) plunging motion.

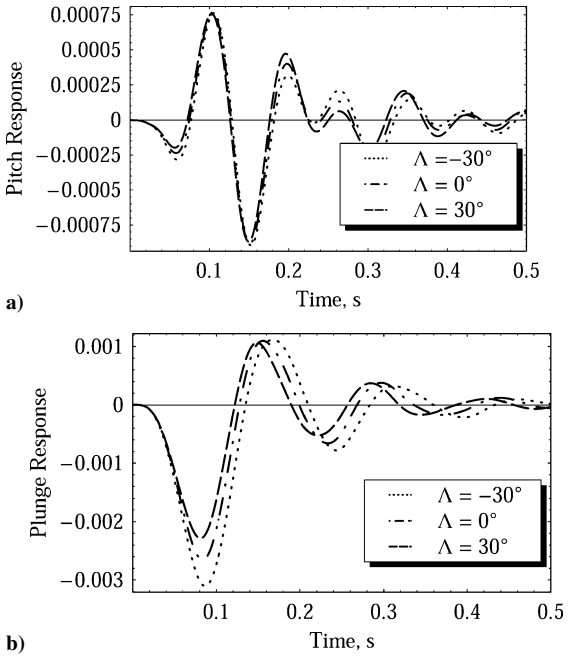

Fig. 13 Effect of sweep angle: a) pitching and b) plunging motion.

k_3/k_1 appears as a multiplicative coefficient in the expression of the temperature field.

Figures 8 and 11–13 show the time histories of the pitch and plunge variables for three different heat flux time periods, four flight speeds, three different transverse shear ratios, and three different sweep angles. Note that in all of these cases, the plunge displacement starting from zero increases in the negative sense and features an oscillatory character. This is consistent with the assumption that the laser impacts the wing on its upper surface, thus, extending the fibers of the upper surface and so determining, in the instant times immediately subsequent to the application of the load, a negative deflection of the wing. Moreover, with respect to the effect of the transverse shear flexibility, note that an increase of it yields a decay of natural frequencies, and, thus, one may expect that the increase of the transverse flexibility would determine an increase of the maximum displacement in both the pitch and plunge motions. However, if the transverse flexibility is increased, this means that the normal does not remain normal after the deformation, hence, during the

motion, part of the energy that would be employed to curve the reference axis of the wing is instead expended to rotate the fibers with respect to the normal. In contrast, this type of flexibility that can be interpreted as the relaxation of the Euler–Bernoulli model affects the torsional behavior in an opposite way. Indeed, now each fiber (or section) of the wing receives less opposition to its torsional motion from the preceding and succeeding fibers. These considerations explain why in Figs. 12 the increase of the transverse shear flexibility yields an increase in the pitch and a slight decrease of the plunge displacements.

Moreover, note that in Fig. 11 the approach of the dynamic response in the time domain has been used also to capture the occurrence of the flutter instability. Indeed, in Fig. 11, for $U_n = 150$ m/s, the forced oscillations, especially for the pitch displacement, exhibit a divergent behavior, suggesting that the wing is already in an unstable flight speed regime and, thus, confirming the results listed in Table 2 related to the WR wing model with transverse shear flexibility $R = 100$, where it was stated that the flutter speed is $V_{\text{flutter}} = 139.6$ m/s. Finally, as highlighted in Fig. 13, for negative Λ, that is, forward-swept wings, an increase and shift of the displacement amplitudes of the plunge time-history toward larger times is experienced.

IX. Conclusions

In this paper, a study of the aerothermoelastic response of rectangular swept wing impacted by a laser beam on its upper surface, made of advanced material and incorporating a number of nonclassical effects, has been presented. In this context, a number of issues have been addressed. According to the obtained results, displayed in the paper, the laser impact affects dramatically the aerothermoelastic response of the aircraft wing, and the induced oscillations can accelerate the failure by fatigue of the structure. In addition, it was shown that the pyrolytic graphite, due to its transversely thermoelastic properties, can be very instrumental toward reducing the induced oscillations of the wing. Moreover, an efficient and accurate solution methodology has been developed. A number of nonclassical effects, such as the transverse shear flexibility and the warping restraint, have been included, and their influence on the aeroelastic characteristics of a simple model have been evaluated. Given the importance of the study initiated here, additional effects are contemplated for inclusion in future works. In particular, the effect of the thermoelastic coupling that represents, in fact, a temperature elastic feedback will be addressed, and the effect of a multilayer structure with thin coatings as external layers for thermal insulation will be considered in our future work.

Acknowledgments

This paper is partially supported by the Italian Space Agency, Grant I/R/253/03. G. M. Polli and F. Mastroddi dedicate this paper to the memory of our teacher, colleague, and friend Chiara Valente.

References

[1]Karpouzian, G., and Librescu, L., "Comprehensive Model of Anisotropic Composite Aircraft Wings Suitable for Aeroelastic Analyses," *Journal of Aircraft*, Vol. 31, No. 3, 1994, pp. 703–712.

[2]Karpouzian, G., and Librescu, L., "Exact Flutter Solution of Advanced Composite Swept Wings in Various Flight Speed Regimes," AIAA Paper 95-1382, April 1995.

[3]Karpouzian, G., and Librescu, L., "Nonclassical Effects on Divergence and Flutter of Anisotropic Swept Aircraft Wings," *AIAA Journal*, Vol. 34, No. 4, 1996, pp. 768–794.

[4]Gern, F. H., and Librescu, L., "Static and Dynamic Aeroelasticty of Advanced Aircraft Wings Carrying External Stores," *AIAA Journal*, Vol. 36, No. 7, 1998, pp. 1121–1129.

[5]Garber, A. M., "Pyrolytic Materials for Thermal Protection Systems," *Aerospace Engineering*, Jan. 1963, pp. 126–137.

[6]Nolan, E. J., and Scala, S. M., "Aerothermodynamic Behavior of Pyrolytic Graphite During Sustained Hypersonic Flight," *ARS Journal*, Vol. 32, No. 1, 1962, pp. 26–35.

[7]Polli, G. M., Librescu, L., and Mastroddi, F., "Aeroelastic Response of Composite Aircraft Swept Wings Impacted by a Laser Beam," AIAA Paper 2004-2046, 2004.

[8]Polli, G. M., *Structural Modeling for Aerothermoelastic Analysis and Control*, Ph.D. Dissertation, School of Aerospace Engineering, Univ. of Rome "La Sapienza," Rome, March 2005.

[9]Boley, B. A., and Weiner, J. H., *Theory of Thermal Stresses*, Wiley, New York, 1960.

[10]Carslaw, H. S., and Jaeger, J. C., *Conduction of Heat in Solids*, Oxford Univ. Press, New York, 1959.

[11]Wei, Z. G., and Batra, R. C., "Deformations of an Axially Loaded Thermoviscoplastic Bar Due to Laser Heating," *Journal of Thermal Stresses*, Vol. 26, No. 7, 2003, pp. 701–712.

[12]Arias, I., and Achenbach, J. D., "Thermoelastic Generation of Ultrasound by Line-Focused Laser Irradiation," *International Journal of Solids and Structures*, Vol. 40, No. 25, 2003, pp. 6917–6935.

[13]Carlson, D. E., "Linear Thermoelasticity," *Encyclopedia of Physics*, edited by C. Truesdell, Vol. VIa/2, Springer-Verlag, Berlin, 1972, pp. 297–345.

[14]Byron, F. W., and Fuller, R. W., *Mathematics of Classical and Quantum Physics*, 2nd ed., Dover, Mineola, NY, 1992.

[15]Thornton, E. A., *Thermal Structures for Aerospace Applications*, AIAA, Reston, VA, 1996.

[16]Bisplinghoff, R. L., Ashley, H., and Halfman, R. L., *Aeroelasticity*, Dover, Mineola, NY, 1996.

[17]Fung, Y. C., *An Introduction to the Theory of Aeroelasticity*, Dover, Mineola, NY, 1969.

[18]Marzocca, P., Librescu, L., and Silva, W. A., "Aeroelastic Response and Flutter of Swept Aircraft Wings," *AIAA Journal*, Vol. 40, No. 5, 2002, pp. 801–812.

[19]Simo, J., and Vu-Quoc, L., "A Geometrically-Exact Rod Model Incorporating Shear and Torsion-Warping Deformation," *International Journal of Solids and Structures*, Vol. 27, No. 3, 1991, pp. 371–393.

[20]Goland, M., "The Flutter of a Uniform Cantilever Wing," *Journal of Applied Mechanics*, Vol. 12, No. 4, 1945, pp. A197–A208.

[21]Goland, M., and Luke, Y. L., "The Flutter of a Uniform Wing with Tip Weights," *Journal of Applied Mechanics*, Vol. 15, No. 1, 1948, pp. 13–20.

[22]Lottati, I., "Flutter and Divergence Aeroelastic Characteristics for Composite Forward Swept Cantilevered Wing," *AIAA Journal*, Vol. 22, No. 11, 1985, pp. 1001–1007.

[23]GE Advanced Ceramics, "Pyrolytic Graphite Brochure," URL: http://www.advceramics.com/geac/products/pyrolytic_graphite/, 2004.

C. Pierre
Associate Editor